2023-07-15

Power performance of an asymmetric wave energy converter near a partial reflection wall

Zhou, B

Title:

Power performance of an asymmetric wave energy converter near a partial reflection wall

Journal:
Ocean Engineering

Author names and affiliations:
Binzhen Zhou[a], Qi Zhang[a], Jianjian Hu[a], Peng Jin[b,d,*], Hengming Zhang[a], Siming Zheng[c,d]

a School of Civil Engineering and Transportation, South China University of Technology, Guangzhou 510641, China
b School of Marine Science and Engineering, South China University of Technology, Guangzhou 511442, China
c School of Engineering, Computing and Mathematics, University of Plymouth, Drake Circus, Plymouth PL4 8AA, UK
d State Key Laboratory of Coastal and Offshore Engineering, Dalian University of Technology, Dalian, 116024, China

* Email address for correspondence: jinpeng@scut.edu.cn (P. Jin)

Power performance of an asymmetric wave energy converter near a partial reflection wall

Binzhen Zhou[a], Qi Zhang[a], Jianjian Hu[a], Peng Jin[b,d,*], Hengming Zhang[a], Siming Zheng[c,d]

[a] *School of Civil Engineering and Transportation, South China University of Technology, Guangzhou 510641, China*

[b] *School of Marine Science and Engineering, South China University of Technology, Guangzhou 511442, China*

[c] *School of Engineering, Computing and Mathematics, University of Plymouth, Drake Circus, Plymouth PL4 8AA, UK*

[d] *State Key Laboratory of Coastal and Offshore Engineering, Dalian University of Technology, Dalian, 116024, China*

Abstract

Wave power absorption of a heaving-body wave energy converter (HBWEC) can be improved by making the device highly asymmetric and deploying it near a coastal wall, harbour pier, or breakwater. However, the coupling between the geometric asymmetry of the HBWEC and the partial reflecting boundaries of the various walls and the consequential influence on the power performance of the HBWEC are unclear. This research aims to fill this gap. A semi-analytical model based on the linear potential flow theory is proposed to deal with an HBWEC with an arbitrary bottom shape and a partial reflection wall. The degree of asymmetry (DoA) of the HBWEC and the reflection rate of the wall are mathematically defined. Results show that the wall increases the power performance of an HBWEC by increasing the reflected wave energy through an increase in the reflection rate. Practically, an HBWEC should have a larger DoA to make it more immune to the change of the reflection rate and therefore more adaptable to different situations. These findings could offer recommendations for the design and deployment of an HBWEC according to the properties of the wall, improving wave power absorption efficiency and avoiding unnecessary costs due to improper design.

Keywords: wave energy converter, asymmetry, wave energy conversion efficiency, partial reflection wall, reflection rate

1. Introduction

In the past few years, the study of wave energy thrives with the rise of a global consensus of transitioning to a low-carbon economy. Various wave energy converters (WECs) have been invented [1]. Among them, the ones using a wave-excited heaving body [2]-[4] to drive a generator are flexible and adaptable and can be applied in niche markets, such as to power buoys of different usages, desalination plants and harbours [5]. Despite the promising prospect, the application of these heaving-body wave energy converters (HBWECs) is hindered by unsatisfactory efficiency and high cost caused by the immaturity of technology [6]. Improvements in the power take-off (PTO) system, such as developing a new generator [7] and using control [8] have been extensively studied. Moreover, the efficiency of an HBWEC highly depends on its hydrodynamic performance [9], which is influenced by three key factors

---

including the shape of the floating body [10], the local wave height [11] and the incident wave frequency [12]. Consequently, researchers worked to optimize the shape of HBWECs and focus high waves for better wave energy conversion.

In two-dimension (2D), the theoretical upper limit of efficiency of a symmetric HBWEC is 50% [13] regardless of the choice of PTO system. The only way to overcome the efficiency limit is to use an asymmetric shape [13]. Madhi *et al*. [14] proposed a Berkeley Wedge HBWEC with a highly asymmetric and peculiar shape and achieved an efficiency of 96.34% after optimizing the PTO damping. Zhang *et al*. [4] carried out a comparative study on three asymmetric PTO-integrated breakwaters [15] with different bottom shapes and found that the use of a simple triangle-baffle configuration can obtain an efficiency of up to 93%. Chen *et al*. [16] optimized the cross-section of a PTO-integrated breakwater by modifying its symmetric structure by replacing the rectangular corner on the seaward side with a circular arc corner. The efficiency was greatly improved whereas the wave attenuation ability was slightly weakened. While the above studies focused on the optimization of individual devices, Zhou *et al*. [17] provided a general explanation of and quantified the influence of asymmetry on efficiency by introducing two mathematical concepts, namely the degree of asymmetry (DoA) and absolute asymmetry, and revealed the role of asymmetry in the proportion of absorbed and reflected wave energy.

HBWECs can be deployed on the seaward side of a coastal wall, harbour pier, or breakwater [18][20]. In such combinations, the coastal wall, harbour pier, or breakwater can disturb the surrounding wave field and focus high waves for the HBWECs through various mechanisms [21]. They can also provide an installation basis for the HBWECs [21] [22]. Zhang *et al*. [23] studied a box-type floating breakwater-Wave Energy Converter (WEC) deployed in front of a total reflection coastal wall. They theoretically predicted the occurrence of the piston mode and sloshing mode resonances of waves between the WEC and the coastal wall and the accompanied increment of efficiency. Sarkar *et al*. [24] studied an Oscillating Wave Surge Converter (OWSC) near a vertical perfect reflection coast. They found when the device was located very close to the coast, the efficiency was much higher than it would be in an open sea. It is indicated in both refs. [23] and [24] that the WEC should not be located at the antinode of standing waves, which could lead to zero efficiency. Zhang *et al*. [25] investigated a hybrid system consisting of an HBWEC and a floating breakwater. They found the wave resonance in the narrow gap between the HBWEC and the breakwater increases the efficiency of a symmetric HBWEC but reduces the efficiency of an asymmetric HBWEC.

The above investigations can be abstracted as the problem of an HBWEC with an arbitrary bottom shape deployed near a wall with a reflection rate $K_{\mathrm{R\_wall}}$ ranging from 0 to 1. $K_{\mathrm{R\_wall}} = 0$ means the wave energy is all dissipated by the wall or there is no wall. $K_{\mathrm{R\_wall}} = 1$ means the wave is perfectly reflected. $0 < K_{\mathrm{R\_wall}} < 1$ means a partial reflection. Although the problem has long been modelled and investigated,

in most cases K_{R_wall} is 0 or 1. As walls are not always perfectly reflecting, the situations where $0 < K_{R\_wall} < 1$ are much more common [26][27] but rarely studied. To model the partial reflection wall, Isaacson *et al.* [26] used a mixed boundary condition instead of the perfect reflection condition based on the study of Berkhoff *et al.* [27], involving a complex transmission coefficient estimated from the conventional reflection coefficient, the reflection phase angle and the incident wave direction. This mixed boundary method was derived only for the propagating mode, whereas the evanescent modes are neglected. The partial reflection boundary conditions were further used by Elchahal *et al.* [28] to study the influence of the reflection rate of the harbour sidewall on the performance of the floating breakwater. Zhao *et al.* [29] extended the work and studied an interconnected floating breakwater-WEC system deployed in front of a porous seawall. They found that the presence of the seawall led to periodical spikes in the frequency domain efficiency curve and the greater the reflection rate the sharper the spikes.

From the literature, the problem of an HBWEC deployed near a wall has been well-studied for individual cases. The conditions where a particular HBWEC can achieve maximum efficiency and where should be avoided as it absorbs little wave energy have been analyzed. The influence of the two key factors, the asymmetry of the HBWEC and the reflection rate of the wall, was also studied but in a separate manner. In most studies of the asymmetry of the HBWEC, the wall was not considered. In the few studies of partial reflection walls, only symmetric HBWECs were involved. Despite the extensive investigations on this topic, the fundamental problem that how to select a proper HBWEC according to the reflecting wall is not answered, since the coupling between the symmetry of the HBWEC and the reflection rate of the wall and its influence on the power performance of the HBWEC are unclear. This is partly due to the lack of a comprehensive model, particularly for such a problem. This study aims to fill these knowledge gaps and its novelties are as follows. First, a comprehensive semi-analytical model able to deal with an HBWEC with an arbitrary bottom shape and a partial reflection wall, which was not accomplished in previous studies, is established. It further involves the evanescent modes, which were ignored in previous models as recognized as unimportant. Here the evanescent modes are shown to be important and cannot be neglected while the HBWEC is close to the wall. Failure of considering them will lead to inaccuracy in computation and non-conservation of energy. Second, the influence of asymmetry of the HBWEC, the reflection rate of the wall and their coupling are investigated to reveal the underlying physics. The findings could help offer recommendations for the design and deployment of HBWECs according to the properties of coastal walls, harbour piers, or breakwaters. Such guidelines should furnish theoretical insights and practical applications to improve wave energy conversion efficiency and avoid unnecessary spending due to improper design.

The rest of the paper is structured as follows. In Section 2, the mathematical model describing the interactions between waves and an HBWEC with an arbitrary bottom shape deployed near a partial reflection wall is given. The definition of the degree of asymmetry and absolute asymmetry of the

HBWEC are also revisited. In Section 3, the present model is validated through a comparison of hydrodynamic coefficients with published results and a test of energy conservation. A comparison between the wall reflection boundary conditions in the present model and previous models is also conducted to show that the evanescent modes cannot be neglected. In Section 4, the optimal location for the deployment of the HBWEC is searched and then the coupling between the asymmetry of the HBWEC and the reflection rate of the wall is investigated. In Section 5, conclusions are drawn.

2. Mathematical model

2.1. System description

A two-dimensional (2D) HBWEC near a partial reflection wall is shown in Figure 1. Same as in refs. [4][22][25][30], the WEC is allowed for heave motion only and moorings are not used. The PTO system with one end connecting to the WEC and the other to the seabed is idealized as linear damping. Wave power is generated by the heave motion of the WEC [4][25]. A global Cartesian coordinate system oxz is adopted with its origin located at the intersection of the calm water surface and the float's vertical central line while the system is in equilibrium. The water depth is h. The immersed part of the float is bounded by two vertical sides at $x = \pm w^{\mathrm{B}}/2$ and a bottom characterized by $z = -d(x)$ for $|x| \le w^{\mathrm{B}}/2$. The distance between vertical central line of WEC and the wall is denoted as D.
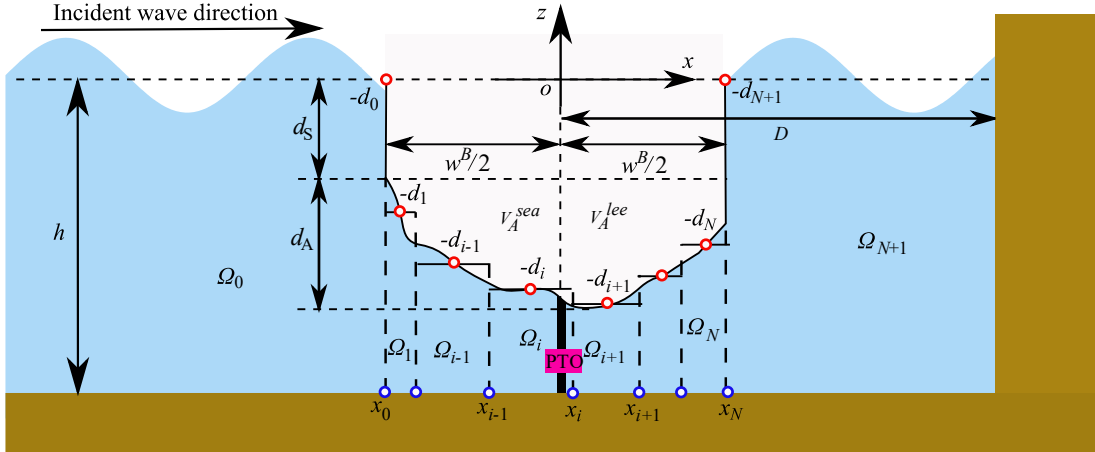

Figure 1 A diagram of an asymmetric HBWEC near a partial reflection wall

The concept of the degree of asymmetry (DoA) [17] is used to characterize the geometric asymmetry of a WEC. As shown in Figure 1, $V_{\mathrm{S}} = d_{\mathrm{S}} w^{\mathrm{B}}$ and d_{S} are the displacement and draft of the symmetric part, respectively. $V_{\mathrm{A}} = \int_{-w^{\mathrm{B}}/2}^{w^{\mathrm{B}}/2} d(x)\mathrm{d}x - d_{\mathrm{S}} w^{\mathrm{B}}$ and d_{A} are the displacement and draft of asymmetric part, respectively. V_{A} is also the sum of the part on the seaward side of the central line with a displacement of $V_{\mathrm{A}}^{\mathrm{sea}}$ and the part on the lee side of the central line with a displacement of $V_{\mathrm{A}}^{\mathrm{lee}}$. The DoA of the WEC is defined as [17]

$$\gamma = \gamma_1 \cdot \gamma_2, \tag{1}$$

$$\gamma_1 = d_A / w^B \tag{2}$$

$$\gamma_2 = \left(V_A^{\text{lee}} - V_A^{\text{sea}}\right) / \left(V_A^{\text{lee}} + V_A^{\text{sea}}\right) \tag{3}$$

where w^B is the width of the WEC. The absolute asymmetry of the WEC is defined as $|\gamma|$.

2.2. Hydrodynamic model

The float is subjected to a regular wave train with an angular frequency ω travelling in the positive x-direction. In the linear potential flow theory, the water flow is described by the velocity potential

$$\phi(x, z, t) = \text{Re}\left[\varphi(x, z)e^{-i\omega t}\right], \tag{4}$$

where $i = \sqrt{-1}$ is the imaginary unit and t denotes time. $\varphi(x, z)$ is the time-independent complex spatial velocity potential that satisfies Laplace's equation,

$$\partial_{xx}\varphi + \partial_{zz}\varphi = 0 \tag{5}$$

φ could be decomposed into scattering and radiation potentials, i.e., $\varphi = \varphi_0 - i\omega\xi_3\varphi_3$. The scattering potential φ_0 is the sum of the incident potential φ^I and the diffraction potential φ^D. ξ_3 is the amplitude of heave motion. φ_3 is the radiation potential due to the heave motion with unit velocity. φ satisfies the following linearized boundary conditions,

$$g\partial_z\varphi = \omega^2\varphi, \text{ on the free surface } z = 0 \tag{6}$$

$$\partial_z\varphi = 0, \text{ on the seabed } z = -h \tag{7}$$

$$\partial_n\varphi_0 = 0, \ \partial_n\varphi_3 = n_3, \text{ on the fluid-float interface} \tag{8}$$

$$\varphi^D, \ \varphi_3 \text{ outgoing: finite value, in the far-field } x \to -\infty \tag{9}$$

$$\partial_x\phi = \alpha k\phi, \ x = x_{\text{wall}} \tag{10}$$

where g is the acceleration of gravity, $\vec{n}$ is the unit normal vector on the fluid-float interface, pointing into the float. n_3 is the component of the unit normal vector in heave mode. k is the wave number with k_0 for the propagating mode and $k_m, \ m = 1, 2, \ldots$ the evanescent modes. The partial reflection boundary condition given in Eq. (10) is introduced by Isaacson and Qu [26]. α is regarded as a complex transmission coefficient and has only been derived for the propagating mode in their study. This will cause inaccuracy in calculation while the WEC is close to the wall as will be shown in Section 3. Here we give the complete form of α for both the propagating mode and evanescent modes.

A general expression of the velocity can be written as follows [13]

$$\phi = \begin{pmatrix} B_0 e^{ik_0(x-x_{\text{wall}})} \\ +C_0 e^{-ik_0(x-x_{\text{wall}})} \end{pmatrix} Z_0(k_0 z) + \sum_{m=1}^{\infty} \begin{pmatrix} B_m e^{-k_m(x-x_{\text{wall}})} \\ +C_m e^{k_m(x-x_{\text{wall}})} \end{pmatrix} Z_m(k_m z) \tag{11}$$

where B_0, C_0, B_m and C_m are unknown coefficients to be determined and can be used to represent the amplitudes of the incident and reflective waves. Substituting Eq. (11) into Eq. (10), we have

$$ik_0(B_0 - C_0)Z_0(k_0 z) - \sum_{m=1}^{\infty} k_m(B_m - C_m)Z_m(k_m z)$$
$$= [\alpha_0 k_0(B_0 + C_0)Z_0(k_0 z) + \sum_{m=1}^{\infty} \alpha_m k_m(B_m + C_m)Z_m(k_m z)] \tag{12}$$

Multiply both sides of Eq. (12) by the eigenfunction and integrate it over the partial reflection wall,

$$ik_0(B_0 - C_0) = \alpha k_0(B_0 + C_0) \tag{13}$$

$$-k_m(B_m - BC_m) = \alpha_m k_m(C_m + C_m) \tag{14}$$

Here the same reflection rate of the wall is assumed for the propagating and evanescent waves, which can be defined as the ratio of incident and reflective wave amplitudes on the wall

$$K_{\text{R\_wall}} = C_0/B_0 = C_m/B_m \tag{15}$$

where $K_{\text{R\_wall}} = 0$ means the incident wave energy is dissipated, $K_{\text{R\_wall}} = 1$ means the incident wave is perfectly reflected and $0 < K_{\text{R\_wall}} < 1$ means a partial reflection. Goda [31] has provided a suggestion about the ranges of reflection rates of a collection of different coastal structures. In the following analysis of the influence of the reflection rate of the wall, $K_{\text{R\_wall}}$ is pre-set as several specific values from 0 to 1. By manipulating Eq. (13) and (14), we have

$$\alpha = \begin{cases} i\dfrac{1-K_{\text{R\_wall}}}{1+K_{\text{R\_wall}}} & \text{Propagating mode} \\ -\dfrac{1-K_{\text{R\_wall}}}{1+K_{\text{R\_wall}}} & \text{Evanescent modes} \end{cases} \tag{16}$$

The incident velocity potential is [32],

$$\varphi^I = -\frac{igA}{\omega}\frac{\cosh[k_0(z+h)]}{\cosh(k_0 h)}e^{ik_0(x-x_0)} \tag{17}$$

where A is the wave amplitude and k_0 obeys the dispersion relation $\omega^2 = gk_0 \tanh(k_0 h)$.

To adopt the semi-analytical approach, the bottom is approximated by discretization into a number (N) of rectangular steps. The ith step begins from $x = x_{i-1}$ to $x = x_i$ with a draft $d_i = d([x_{i-1} + x_i]/2)$, $i = 1, \dots, N$. Note that $x_0 = -w^B/2$ and $x_N = w^B/2$, and let $d_0 = d_{N+1} = 0$. The fluid domain is divided into $N + 2$ columns: Ω_0 for $x < x_0$ and $-h < z < -d_0$, Ω_i for $x_{i-1} < x < x_i$ and $-h < z < -d_i$, $i = 1, \dots, N$, and Ω_{N+1} for $x_N < x < x_{\text{wall}}$ and $-h < z < d_{N+1}$, where x_{wall} denotes the position of the partial reflection wall. From Eqs. (5)-(9) and using the separation of variables, the velocity potential in each subdomain could be given according to refs. [33]-[35]. For $i = 1, \dots, N$ and $j = 0, 3$,

$$\varphi_j^{\Omega_0} = \delta_{0j}\varphi^I + \left(-\frac{igA}{\omega}\right)^{\delta_{0j}} \begin{bmatrix} R_{0j}^{\Omega_0}e^{-ik_0(x-x_0)}Z_0(z) + \\ \sum_{m=1}^{\infty} R_{mj}^{\Omega_0}e^{k_m(x-x_0)}Z_m(z) \end{bmatrix} \tag{18}$$

6

$$\varphi_j^{\Omega_i} = \left(-\frac{igA}{\omega}\right)^{\delta_{0j}} \begin{bmatrix} \varphi_j^{p,\Omega_i} + \left(S_{0j}^{\Omega_i} + T_{0j}^{\Omega_i}x\right)Y_0^{\Omega_i}(z) + \\ \sum_{l=1}^{\infty}\left(S_{lj}^{\Omega_i}e^{\lambda_l^{\Omega_i}x} + T_{lj}^{\Omega_i}e^{-\lambda_l^{\Omega_i}x}\right)Y_l^{\Omega_i}(z) \end{bmatrix} \tag{19}$$

$$\varphi_j^{\Omega_{N+1}} = \left(-\frac{igA}{\omega}\right)^{\delta_{0j}} \begin{bmatrix} R_{0j}^{\Omega_{N+1}}\left(e^{ik_0(x-x_N)} + K_{\text{R\_wall}}e^{-ik_0(x+x_N-2x_{\text{wall}})}\right)Z_0(z) + \\ \sum_{m=1}^{\infty}R_{mj}^{\Omega_{N+1}}\left(e^{-k_m(x-x_N)} + K_{\text{R\_wall}}e^{k_m(x+x_N-2x_{\text{wall}})}\right)Z_m(z) \end{bmatrix} \tag{20}$$

where δ is the Kronecker Delta function. $\delta = 1$ when the two indices in the subscript are equal and $\delta = 0$ otherwise. $R_{0j}^{\Omega_0}$, $R_{mj}^{\Omega_0}$, $S_{0j}^{\Omega_i}$, $S_{lj}^{\Omega_i}$, $T_{0j}^{\Omega_i}$, $T_{lj}^{\Omega_i}$, $R_{0j}^{\Omega_{N+1}}$ and $R_{mj}^{\Omega_{N+1}}$ ($m, l = 1, 2,...$) are unknowns to be determined. In Ω_0 and Ω_{N+1}, k_m ($m = 1, 2,...$) obeys the dispersion relation $\omega^2 = -gk_m\tan(k_mh)$[36]. The corresponding eigenfunctions $Z_0(z)$ and $Z_m(z)$ are defined as

$$Z_0(z) = \frac{\cosh[k_0(z+h)]}{\cosh(k_0 h)}, \ Z_m(z) = \frac{\cos[k_m(z+h)]}{\cos(k_m h)} \tag{21}$$

$\lambda_0^{\Omega_i}$ and $\lambda_l^{\Omega_i}$ ($l = 1, 2, ...$) are the eigenvalues in the subdomain Ω_i. Subjected to the homogeneous boundary conditions on the seabed (Eq. (7)) and the bottom of the asymptotic float while it is in equilibrium,

$$\partial_z\varphi = 0, \text{ on the bottom of the asymptotic float } z = -d_i \tag{22}$$

$\lambda_0^{\Omega_i}=0$ and $\lambda_l^{\Omega_i} = l\pi/(h - d_i)$. The corresponding eigenfunctions $Y_0^{\Omega_i}(z)$ and $Y_l^{\Omega_i}(z)$ are

$$Y_0^{\Omega_i}(z) = \frac{\sqrt{2}}{2}, \ Y_l^{\Omega_i}(z) = \cos[\lambda_l^{\Omega_i}(z + h)] \tag{23}$$

φ_j^{p,Ω_i} is a solution of radiation potential in Ω_i satisfying the non-homogeneous condition in Eq. (8). Based on refs. [33]-[35], it is expressed as

$$\varphi_j^{p,\Omega_i} = \frac{(z+h)^2 - x^2}{2(h-d_i)}\delta_{3j} \tag{24}$$

The continuity conditions are used to determine the unknown coefficients $R_{0j}^{\Omega_0}$, $R_{mj}^{\Omega_0}$, $S_{0j}^{\Omega_i}$, $S_{lj}^{\Omega_i}$, $T_{0j}^{\Omega_i}$, $T_{lj}^{\Omega_i}$, $R_{0j}^{\Omega_{N+1}}$ and $R_{mj}^{\Omega_{N+1}}$ ($m, l = 1, 2,...$). The specific procedure could be referred to ref. [17].

The first M terms in $R_{mj}^{\Omega_0}$ and $R_{mj}^{\Omega_{N+1}}$ and the first L terms in $S_{lj}^{\Omega_i}$ and $T_{lj}^{\Omega_i}$ are truncated. A linear system of $2(M + 1) + 2N(L + 1)$ complex equations for each j is yielded.

$$\mathbf{AX}_j = \mathbf{B}_j \tag{25}$$

where $\mathbf{X}_j = \left[R_{0j}^{\Omega_0},\dots,R_{Mj}^{\Omega_0},S_{0j}^{\Omega_i},\dots,S_{Lj}^{\Omega_i},T_{0j}^{\Omega_i},\dots,T_{Lj}^{\Omega_i},R_{0j}^{\Omega_{N+1}},\dots,R_{Mj}^{\Omega_{N+1}}\right]^T$. The expressions of most

items in $\mathbf{A}$ and $\mathbf{B}_j$ can be obtained from ref. [17], together with

$$\begin{cases} A_{l,m}^{\Omega_{N+1},p} = \frac{\int_{-h}^{-d_N} 2Z_m(k_m z)Y_l\left(\lambda_l^{\Omega_N}z\right)dz}{(h-d_N)}\left[1 + K_R e^{-2ik_0(x_N-x_{\text{wall}})}\right] \\ A_{0,0}^{\Omega_{N+1},v} = ik_0 Q_0\left[1 - K_{\text{R\_wall}}e^{-2ik_0(x_N-x_{\text{wall}})}\right] \\ A_{m,m}^{\Omega_{N+1},v} = k_m Q_m\left[1 - K_{\text{R\_wall}}e^{2k_m(x_N-x_{\text{wall}})}\right] \end{cases} \tag{26}$$

2.3. Energy conversion efficiency, reflection coefficient and transmission coefficient

The wave excitation force, added mass and radiation damping can be derived according to ref. [17]. The motion response ξ_3 of the WEC could be solved from the equation of motion in the frequency domain

$$\left[-\omega^2(m_{33} + a_{33}) - i\omega\left(b_{33} + b_{33}^{\text{PTO}}\right) + c_{33}\right]\xi_3 = F_3^{\text{EX}} \tag{27}$$

where $m_{33} = \rho V$, a_{33}, b_{33}, b_{33}^{PTO}, and $c_{33} = \rho g S$ are the mass, added mass, radiation damping, PTO damping and hydrostatic restoring stiffness of the float, respectively. F_3^{EX} is the vertical wave excitation force. V is the displacement of the float and $S = w^{\text{B}}$ is the area of the waterplane, i.e., the width of the WEC w^{B}. The motions of the WEC in surge and pitch are restricted by adopting a stiffness of 1.0×10^{30} N/m, only heave motion is released. The time-averaged absorbed power is

$$P^{\text{ave}} = \frac{1}{2}\omega^2 b^{\text{PTO}}|\xi_3|^2 \tag{28}$$

The power per unit incident wave width is [37]

$$P^{\text{wave}} = \frac{1}{4}\rho g A^2 \left[1 + \frac{2k_0 h}{\sinh(2k_0 h)}\right]\frac{\omega}{k_0} \tag{29}$$

The energy conversion efficiency of the PTO-integrated breakwater is

$$\eta = \frac{P^{\text{ave}}}{P^{\text{wave}}} \tag{30}$$

The theoretical optimization of PTO damping can be derived as [38]:

$$b^{\text{opt}} = \frac{1}{\omega}\sqrt{[(m_{33} + a_{33})\omega^2 - c_{33}]^2 + \omega^2 b_{33}^2} \tag{31}$$

The optimal absorbed power can then be computed from Eq. (28).

While the velocity potential is solved, the energy reflected by WEC and the partial reflection wall could be expressed in the form of a reflection coefficient K_R, and the energy dissipated by the partial reflection wall could be expressed in the form of a transmission coefficient K_T

$$K_R = \left|\frac{\varphi^D - i\omega\xi_3\varphi_3}{\varphi^I}\right|_{x=-\infty} = \left|R_{00}^{\Omega_0} + \frac{\omega^2 R_{03}^{\Omega_0}\xi_3}{gA}\right| \tag{32}$$

$$K_T = \sqrt{1 - K_{\text{R\_wall}}^2}\left|\frac{\varphi^I + \varphi^D - i\omega\xi_3\varphi_3}{\varphi^I}\right|_{x=+\infty} = \sqrt{1 - K_{\text{R\_wall}}^2}\left|R_{00}^{\Omega_{N+1}} + \frac{\omega^2 R_{03}^{\Omega_{N+1}}\xi_3}{gA}\right| \tag{33}$$

8

The main nomenclatures are provided in Table 1:

Table 1 Main nomenclatures

Parameter	Symbol	Parameter	Symbol
Degree of asymmetry (DoA)	γ	Water depth	h
WEC draft	l^{B}	Wave number	k
WEC width	w^{B}	Wave frequency	ω
Optimal PTO damping	b^{opt}	Reflection rate of the wall	$K_{\mathrm{R\_wall}}$
Energy conversion efficiency	η	Reflection coefficient	K_{R}
Distance between the WEC and the wall	D	Transmission coefficient	K_{T}

3. Validation

The validation of the present model is two-folded. The semi-analytical approach for the asymptote of the arbitrary bottom of the WEC should be first verified. This has been done in a previous work of the authors (Zhou *et al*. [17]) and will not be repeated here. The presence of the partial reflection wall should also be verified, which is emphasized in the present validation. This is carried out by a two-step procedure. First, the interaction between the WEC and the wall should be validated. The results proposed by Zheng *et al*. [33] are employed for comparison. In their paper, the radiation and diffraction of a 2D rectangular box deployed in front of a seawall were analytically investigated. The comparison is carried out by examining the hydrodynamic coefficients of a rectangular box (width and draft: $w^{\mathrm{B}}/h = 0.33$, $d_{\mathrm{S}}/h = 0.4$) deployed at $D/h = 0.367$ from a wall with $K_{\mathrm{R\_wall}} = 1$. The comparative results are shown in Figure 2. Good agreement is achieved with a maximum difference of 0.83% (the ratio is calculated by the following equation: Difference = |Present-Published|/Published). Then the modelling of the reflection rate of the partial reflection wall and the wave energy conversion of the WEC is validated through a test of energy conservation (Figure 3). A rectangular WEC (width and draft: $w^{\mathrm{B}}/h = 0.33$, $d_{\mathrm{S}}/h = 0.4$) deployed at $D/h = 0.8$ from a wall with $K_{\mathrm{R\_wall}} = 0.6$ is employed. The reflected energy, dissipated energy and absorbed energy are conservative.

A comparison between the mixed boundary conditions in the present model and the previous models is also conducted. The present mixed boundary condition considers the influence of evanescent modes, whereas the previous boundary condition did not. A rectangular WEC (width and draft: $w^{\mathrm{B}}/h = 0.5$, $d_{\mathrm{S}}/h = 0.6$) and a partial reflection wall ($K_{\mathrm{R\_wall}} = 0.5$) are employed. Two cases with $D/h = 0.3$ and $D/h = 1$ are simulated. The PTO damping of the WEC is optimized in each case. The results are shown in Figure 4. When $D/h = 1$, the two models are both accurate. When $D/h = 0.3$, energy is conservative in the present model but is not in previous models. This is because as the WEC and the wall become closer, the influence of the evanescent modes becomes significant and cannot be neglected as in previous models. A further examination of the influence of the evanescent modes concerning the change in the distance between the WEC and the wall is presented in Figure 5.
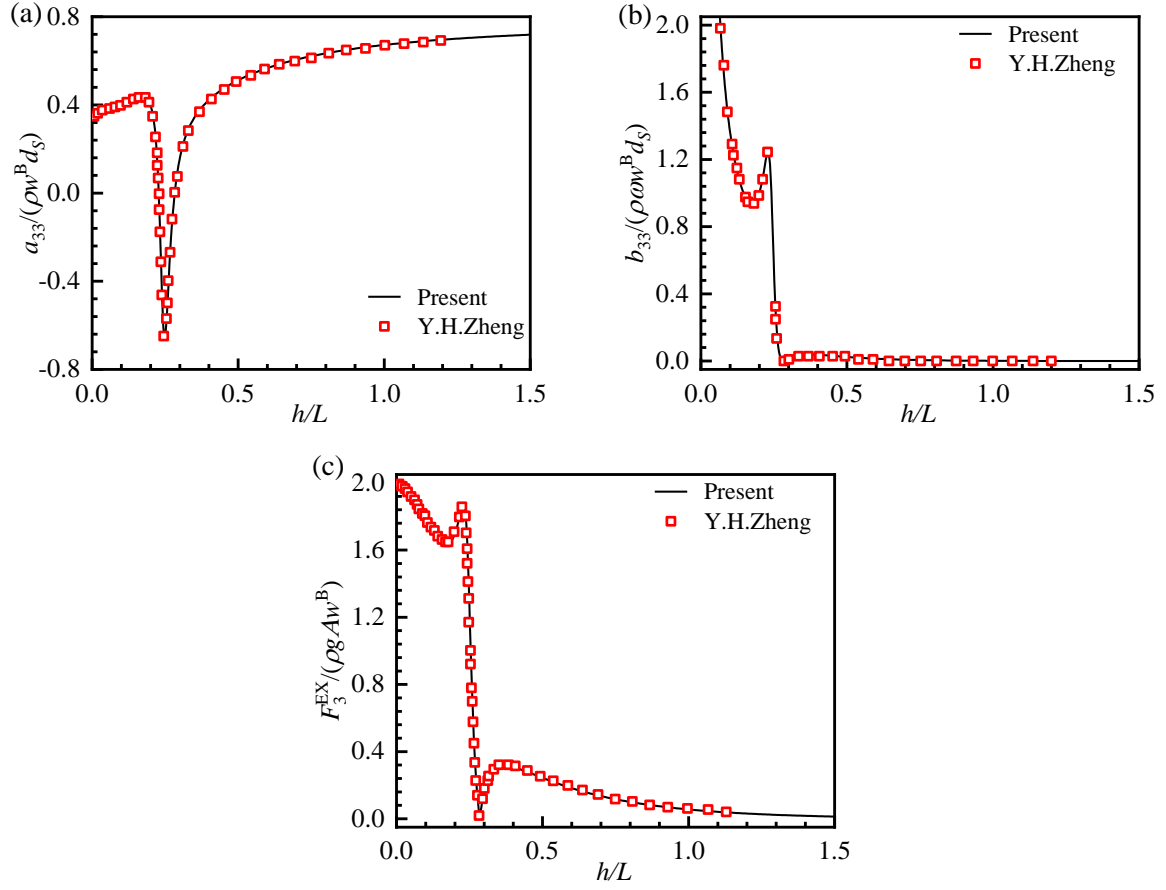
Figure 2 Comparison of hydrodynamic coefficients of a rectangular box in front of a reflective wall:
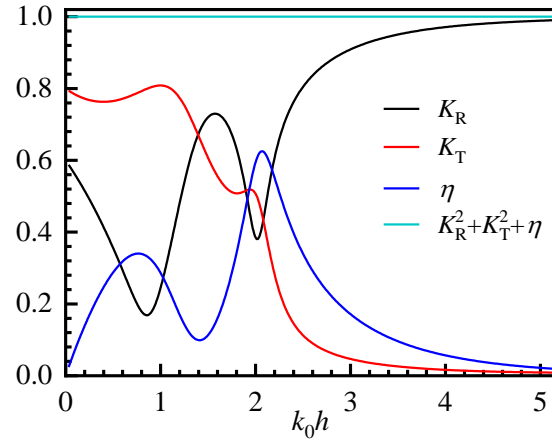(a) added mass; (b) radiation damping; (c) wave excitation force

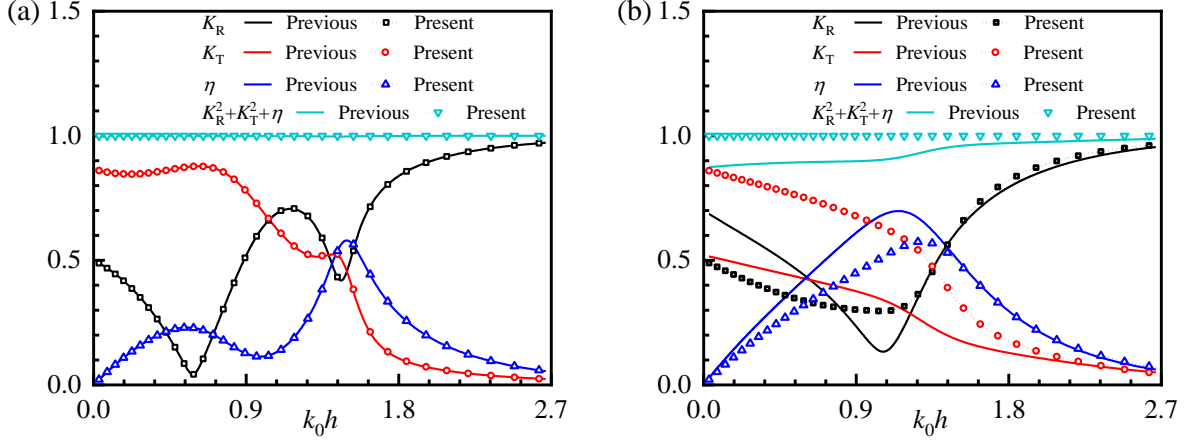Figure 3 Energy conservation test of a rectangular WEC near a partial reflection wall

Figure 4 Energy conservation test of previous and present partial reflection boundary conditions for a rectangular WEC with different D/h: (a) 1; (b) 0.3.
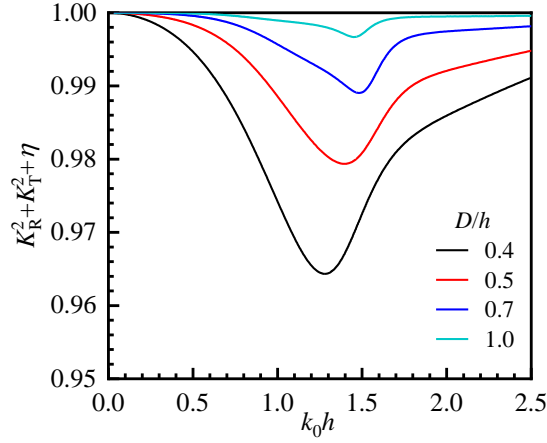

Figure 5 Non-conservation of energy of previous partial reflection boundary condition for a rectangular WEC with different D/h
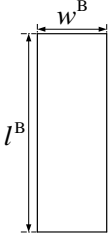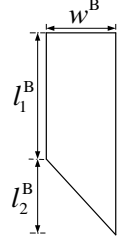
4. Numerical results

In this section, the effects of the asymmetry of the HBWEC, the reflection rate of the wall and their coupling on the power performance of the HBWEC are investigated after the optimal deployment location is determined. The water depth is h=20 m. Regular incident waves with a period ranging from 4 s to 7 s (dimensionless wave number k_0h from 4.93 to 14.85) according to field data of typical China seas [39] are used and their amplitudes are set as unit length. The PTO damping is optimized for all cases according to Eq.(31). The HBWEC can reach an efficiency peak while it is resonant.

4.1. Optimal location for HBWEC

A location where an HBWEC can achieve its optimal power performance is expected to exist regardless of the shape of the HBWEC and the reflection rate of the wall. The two HBWECs used in this investigation are shown in Table 2. WEC #1 is used to search for the optimal location. Its dimensions are $l^B/h = 0.36$ and $w^B/h = 0.09$. The reflection rate of the wall is $K_{R\_wall} = 0.6$. As the frequency of ocean waves always varies, the power performance of an HBWEC is determined not only by the peak

efficiency in a particular frequency but by the power in the entire wave spectrum (4 s to 7 s). Therefore, the integral of efficiency over a wave period from 4 s to 7 s is used as a criterion for comparing power performance. 61 different locations are chosen, including D/h ranging from 0.05 to 3.0 with an increment of 0.05 and $D/h = 0.045$ (closely attached to the wall). The comparative results are given in Figure 6.

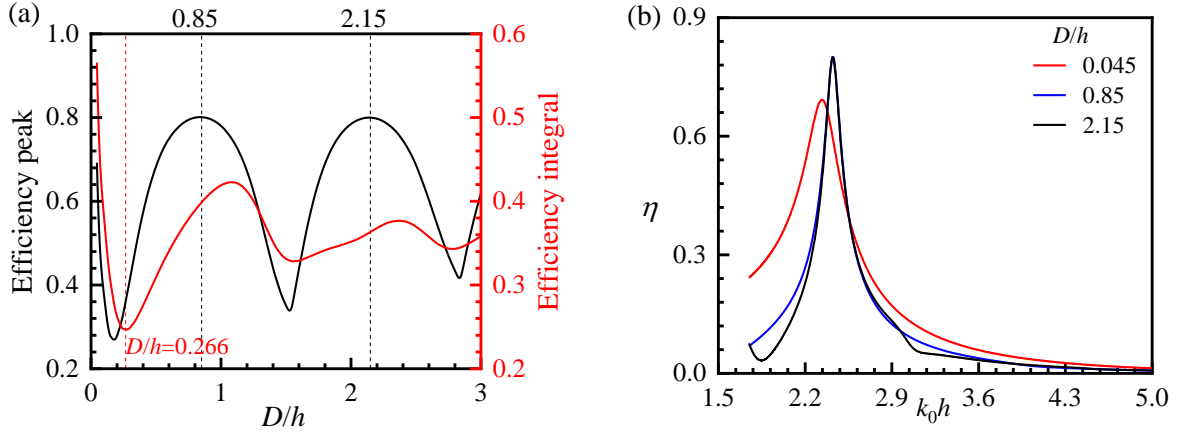Table 2 Configurations of WECs

Models	WEC #1	WEC #2
Cross-section		

Figure 6 Wave energy performance of WEC #1: (a) integral area and maximum value of the efficiency η; (b) the efficiency η corresponding to different D/h.

The efficiency peak and the efficiency integral over the wave spectrum for different D/h are in Figure 6a. The maximum value of the efficiency integral occurs for $D/h = 0.045$, where the HBWEC is attached to the wall with no gap in between. However, the maximum value of the efficiency peak is not obtained at this location. Two greater local maximum values of the efficiency peak occur for $D/h = 0.85$ and $D/h = 2.15$. From a closer examination of the efficiency for $D/h = 0.045$, 0.85 and 2.15 in a range of $k_0 h$ shown in Figure 6b, while the HBWEC is attached to the wall, although the efficiency peak is not the largest, the efficiency band is the broadest. This explains why the maximum value of the efficiency integral does not match the maximum value of the efficiency peak.
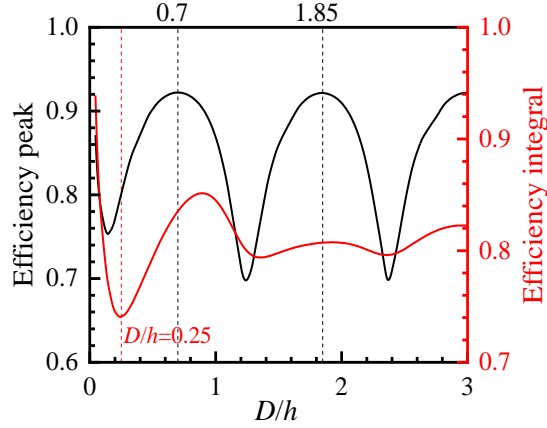
Figure 7 Integral area and maximum value of the efficiency η of WEC #2

The generality of the result is then verified by WEC #2 with different geometry properties deployed at a different place in front of a wall with a different reflection rate. Its dimensions are $l_1^B/h=0.18$, $l_2^B/h=0.18$ and $w^B/h = 0.09$. A wall with $K_{R\_wall} = 0.4$ is employed. The results are shown in Figure 7. The patterns of both the efficiency peak and efficiency integral of WEC #2 are similar to those of WEC #1. The optimal location for WEC #2 is the same as that of WEC #1. From the above results, the most effective way of deploying an arbitrary HBWEC is to closely attach it to the wall without leaving a gap. The HBWEC can benefit from a broader efficiency band due to the presence of the wall. Note that the location where the WEC obtains the worst power performance is also close to the wall (the two first troughs of the efficiency integral shown in Figure 6 and Figure 7). The worst location should be carefully avoided because it is quite near the optimal location.

4.2. Degree of asymmetry of HBWEC

The effect of the DoA of the HBWEC on its power performance under the presence of a wall with various reflection rates is investigated. WECs from #3 to #7 with $\gamma = -1, -0.667, 0, 0.667$ and 1 are used and their configurations are shown in Figure 8 and Table 3. The walls with $K_{R\_wall} = 0, 0.5$ and 1 are employed. Referring to Figure 1, the symmetric (upper) parts of WEC#3~WEC#7 are the same. The displacements of the asymmetric parts of these HBWECs are also the same. The change of DoA is implemented by sliding the vertex of the triangle. In this way, the masses of the five WECs are kept equal and the influence of the difference in their heaving natural periods is utmostly minimized. The change of efficiency against k_0h is presented in Figure 9. The efficiency peaks and their corresponding dimensionless wave number k_0h are given in Table 4 and Table 5, respectively.
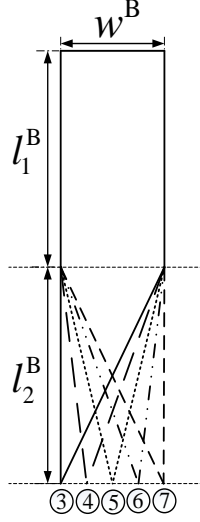
Figure 8 Five HBWECs with equal masses but different DoAs

Table 3 Geometric properties of WECs #3~#7

WEC	l_1^B (m)	l_2^B (m)	l^B (m)	w^B (m)	γ
#3	3.6	3.6	7.2	1.8	−1
#4	3.6	3.6	7.2	1.8	−0.667
#5	3.6	3.6	7.2	1.8	0
#6	3.6	3.6	7.2	1.8	0.667
#7	3.6	3.6	7.2	1.8	1

Table 4 Efficiency peaks of WECs #3~#7

WEC	$K_{R\_wall} = 0$	$K_{R\_wall} = 0.25$	$K_{R\_wall} = 0.5$	$K_{R\_wall} = 0.75$	$K_{R\_wall} = 1$
#3	0.039	N/A	N/A	0.288	1.000
#4	0.203	N/A	0.201	N/A	1.000
#5	0.500	0.442	0.406	0.431	0.999
#6	0.797	N/A	0.709	N/A	0.999
#7	0.960	0.964	0.971	0.983	1.000

Table 5 Dimensionless wave numbers k_0h where the efficiency peaks of WECs #3~#7 are obtained

WEC	$K_{R\_wall} = 0$	$K_{R\_wall} = 0.25$	$K_{R\_wall} = 0.5$	$K_{R\_wall} = 0.75$	$K_{R\_wall} = 1$
#3	3.21	N/A	N/A	2.25	2.28
#4	3.42	N/A	3.10	N/A	2.54
#5	3.47	3.42	3.33	3.11	2.80
#6	3.42	N/A	3.37	N/A	3.03
#7	3.27	3.27	3.25	3.24	3.23

From Figure 9a and Figure 9b, while $K_{R\_wall} \neq 1$, the DoA has a large influence on the efficiency peak and a small influence on the natural period of the HBWEC. An HBWEC with a greater DoA has an absolute advantage in wave energy conversion in the entire wave spectrum. For example, comparing WEC #3 with $\gamma = -1$ and WEC #7 with $\gamma = 1$ for $K_{R\_wall} = 0$. The efficiency of WEC #7 is relatively large

in the wave spectrum and has an efficiency peak of 0.96, whereas WEC #3 absorbs only a little wave energy. Similar results have also been demonstrated in ref. [17] where the wall was not considered. From Figure 9c, for $K_{R\_wall} = 1$, all WECs reach the same efficiency peak $\eta = 1$, but the efficiency bandwidth and the natural period of the HBWECs are quite different. An HBWEC with a greater DoA has a smaller natural period and broader bandwidth. It loses the advantage of a larger efficiency peak but still has a broader efficiency band. One can also obtain $K_R = 0$ according to Eq.(32) while the wall is perfectly reflective and the HBWEC is resonant. In this situation, the reflected wave and radiated wave canceled each other and all energy is absorbed.
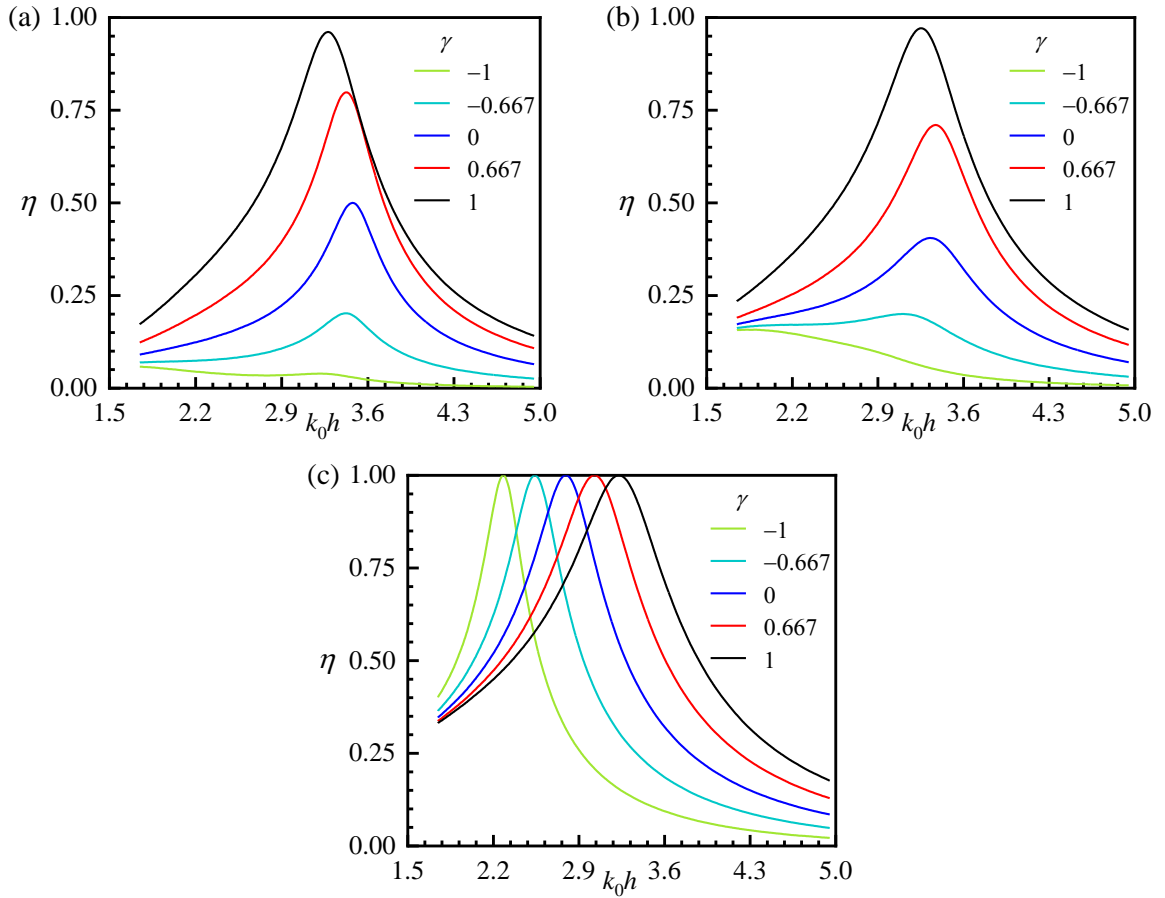

Figure 9 Energy conversion efficiency η of WECs #3~#7, the reflection rates of the walls K_{R_wall}:

(a) 0; (b) 0.5; (c) 1

4.3. Reflection rate of wall

Then the effect of the reflection rate of the wall on the power performance of the HBWEC is investigated. The walls with $K_{R\_wall} = 0$, 0.25, 0.5, 0.75 and 1 and the HBWECs with $\gamma = -1$, 0 and 1 are employed. The change of efficiency against k_0h is presented in Figure 10. The efficiency peaks and their corresponding dimensionless wave number k_0h are given in Table 4 and Table 5, respectively.

From the results in Figure 10a, b and c, generally, an increase in the reflection rate of the wall increases the efficiency of the HBWEC. This is because as the reflection rate of the wall increases, the wave

energy reflected by the wall increases. This part of wave energy could also be absorbed by the HBWEC, which increases the total absorbed power. As revealed by the left shift of the efficiency peak, an increase in the reflection of the wall also increases the natural period of the HBWEC. As the hydrostatic restoration coefficient and the mass of the HBWECs do not change, the increase in natural period indicates that the presence of the wall increases the added mass of the HBWECs [36], and the greater the reflection rate of the wall, the larger the addition to the added mass, as shown in Figure 10d.
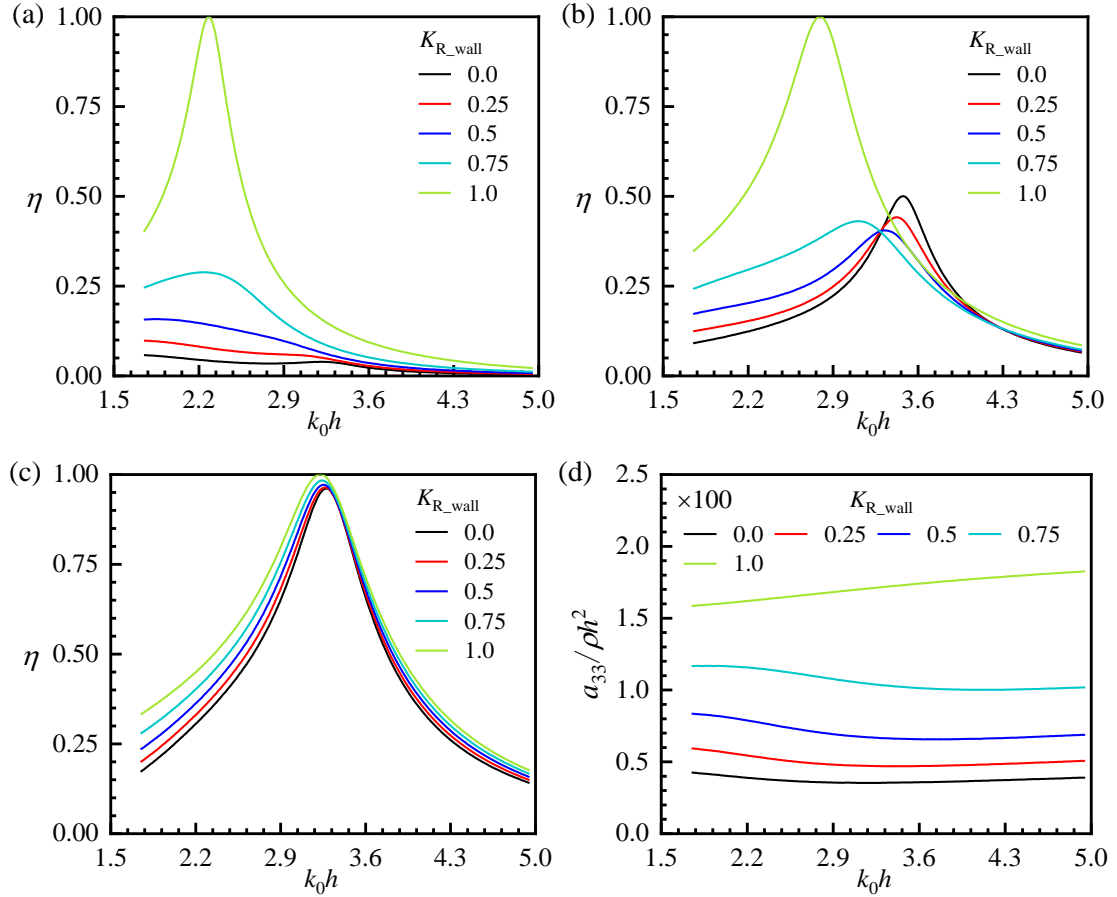

Figure 10 Energy conversion efficiency η of (a) WEC #3; (b) WEC #5; (c) WEC #7 and (d) the dimensionless added mass a_{33} of WECs #3 for K_{R_wall} = 0, 0.25, 0.5, 0.75 and 1.

4.4. Coupling between asymmetry and reflection

From the above analysis, as shown in Figure 9 and Figure 10 and Table 4 and Table 5, both the DoA of the HBWEC and the reflection rate of the wall influence the power performance of the HBWEC, but their influential regions are different. The efficiency of the HBWEC highly depends on its DoA. The reflection rate of the wall determines the amount of the reflected wave energy and increases the added mass of the HBWEC, and a larger reflection rate leads to greater influence. In this section, how the DoA of the HBWEC and the reflection rate of the wall couple with each other and how the coupling influences the power performance of the HBWEC are discussed.

Considering a case that the incident waves interact with the HBWEC, the wave energy is reflected,

absorbed (call this first absorption hereafter) and transmitted by the HBWEC. While $K_{R\_wall} = 0$, the transmitted wave energy will not be reflected and reused in this case. While $K_{R\_wall} \neq 0$, the wave energy transmitted by the HBWEC is dissipated and reflected by the wall, and the proportions of the dissipated and reflected wave energy are determined by the reflection rate of the wall. Part of the wall-reflected wave energy is again absorbed by the HBWEC (call this second absorption hereafter). This can explain why the presence of the wall can almost always increase the efficiency of the HBWEC. Because the energy through the second absorption is complemented, as shown in Figure 10. As found in ref. [17], the amount of wave energy transmitted by the HBWEC changes a little while the draft and the absolute asymmetry of the HBWEC were fixed. That is, while the orientation of an asymmetric HBWEC reverses (the sign of DoA reverses), it only changes the proportions of the reflected and absorbed wave energy but not changes the proportion of the transmitted wave energy. For an HBWEC with a larger DoA, most of the un-transmitted wave energy is extracted through the first absorption. To the waves reflected by the wall, the sign of DoA of the HBWEC reverses and therefore only a small amount of the reflected wave energy is extracted by the second absorption. For an HBWEC with a smaller DoA, the opposite process happens. Most of the un-transmitted wave energy is reflected by the WEC and the first absorption is small. The second absorption could be large depending on the amount of transmitted energy. In summary, while $K_{R\_wall} \neq 1$, the efficiency of an HBWEC with a positive DoA is the sum of a large first absorption and a small second absorption and is dominated by the first absorption. The situation reverses for an HBWEC with a negative DoA and whether the efficiency could be dominated by the second absorption depends on its wave attenuation ability and the reflection rate of the wall. This explains why the efficiency of an HBWEC with a smaller DoA is more easily influenced by a wall with a larger reflection rate. Because in this situation the second absorption becomes more prominent. A special case occurs for $K_{R\_wall} = 1$, where one can obtain $K_R=0$ by Eq.(32). The reflected wave and radiated wave cancelled each other. No wave energy is dissipated and all is absorbed.

The wall also changes the added mass of the HBWEC. From the comparative results in Table 4 and Table 5, while $K_{R\_wall} = 0$, the natural periods of WEC #3 and WEC #7 are close. As K_{R_wall} increases, the natural periods of all HBWECs increase, but the increase of an HBWEC with a smaller DoA is larger. The wall has a larger influence on the added mass of an HBWEC with a smaller DoA. It also has a larger influence on the power performance of an HBWEC with a smaller DoA. It can be concluded that while the DoA of the HBWEC is smaller and the reflection rate of the wall is larger, the power performance of the WEC is more influenced by the wall. This can also be evident in Figure 10. The efficiency of the HBWEC with $\gamma = 1$ is almost not influenced by the change of reflection rate compared with the two HBWECs with $\gamma = -1$ and $\gamma = 0$. From a practical view, as the wall is not always vertical nor is perfectly reflecting, its reflection rate of the wall is mostly $0< K_{R\_wall} <1$, the HBWEC with a larger DoA is more immune to the change of the reflection rate and therefore more adaptable to different situations.

5. Conclusion

A 2D frequency-domain semi-analytical model dealing with an HBWEC with an arbitrary bottom shape deployed in front of a partial reflection wall is established based on the linear potential flow theory. The method of matching eigenfunction is applied to solve the diffracted and radiated potential. The model is validated against published results and demonstrated more comprehensively than previous models by considering the evanescent modes. The concepts of the degree of asymmetry and the absolute asymmetry of the HBWEC and the reflection rate of the wall are mathematically determined. The HBWEC is deployed at different distances to the wall and the corresponding power performances are compared. The coupling between the asymmetry of the HBWEC and the reflection rate of the wall and the consequential influence on the power performance of the HBWEC are investigated. The major conclusions are:

(1) The optimal location for an arbitrary HBWEC to achieve its maximum power performance in the entire wave spectrum is closely attached to the wall.

(2) Similar to the situation without a wall, an HBWEC with a larger DoA has better power performance.

(3) The partial reflection wall influences the power performance of an HBWEC by increasing its added mass and the reflected wave energy through an increase in the reflection rate. This influence is larger on an HBWEC with a smaller DoA.

(4) Practically, the HBWEC should be built with a large DoA to obtain higher power performance and better adaptability to different walls.

The major limitations of the present study are:

(1) Viscous drag is not considered.

(2) Only the potential flow theory of linear waves is used.

(3) Only theoretical derivation is carried out, whereas lab-scale or open-sea experimental study is not conducted to validate the influence of varying DoA and $K_{\text{R\_wall}}$.

(4) Only regular waves are considered.

Future works can be carried out following the points:

(1) Effect of the boundary layers between the WEC and the wall.

(2) Performance of an array of asymmetric HBWECs.

(3) Cost evaluation of wave energy conversion.

(4) Optimization of the HBWEC body geometries.

(5) Influence of varying bathymetry.

Acknowledgement

Reference

[1] Drew, B., Plummer, A. R., & Sahinkaya, M. N. (2009). A review of wave energy converter technology. *Proceedings of the Institution of Mechanical Engineers, Part A: Journal of Power and Energy*, 223(8), 887-902.

[2] Jin, P., Zhou, B., Göteman, M., Chen, Z., & Zhang, L. (2019). Performance optimization of a coaxial-cylinder wave energy converter. *Energy*, 174, 450-459.

[3] Zhou, B. Z., Wang, Y., Hu, J. J., Jin, P., & Wang, L. (2023). Evaluation and optimization of a hybrid wave energy converter using excited motion response in two degrees of freedom. *Journal of Hydrodynamics*, 1-10.

[4] Zhang, H., Zhou, B., Vogel, C., Willden, R., Zang, J., & Zhang, L. (2020). Hydrodynamic performance of a floating breakwater as an oscillating-buoy type wave energy converter. *Applied Energy*, 257, 113996.

[5] Renzi, E., Michele, S., Zheng, S., Jin, S., & Greaves, D. (2021). Niche applications and flexible devices for wave energy conversion: A review. *Energies*, 14(20), 6537.

[6] Zhao, X. L., Ning, D. Z., Zou, Q. P., Qiao, D. S., & Cai, S. Q. (2019). Hybrid floating breakwater-WEC system: A review. *Ocean Engineering*, 186, 106126.

[7] Ahamed, R., McKee, K., & Howard, I. (2022). A Review of the Linear Generator Type of Wave Energy Converters' Power Take-Off Systems. *Sustainability*, 14(16), 9936.

[8] Ozkop, E., & Altas, I. H. (2017). Control, power and electrical components in wave energy conversion systems: A review of the technologies. *Renewable and Sustainable Energy Reviews*, 67, 106-115.

[9] Ning, D., Zhao, X., Göteman, M., & Kang, H. (2016). Hydrodynamic performance of a pile-restrained WEC-type floating breakwater: An experimental study. *Renewable Energy*, 95, 531-541.

[10] Zhou, B. Z., Hu, J. J., Sun, K., Liu, Y., & Collu, M. (2020). Motion response and energy conversion performance of a heaving point absorber wave energy converter. *Frontiers in Energy Research*, 8, 553295.

[11] Zhou, B., Zheng, Z., Jin, P., Wang, L., & Zang, J. (2022). Wave attenuation and focusing performance of parallel twin parabolic arc floating breakwaters. *Energy*, 260, 125164.

[12] Zhou, B., Hu, J., Jin, P., Sun, K., Li, Y., & Ning, D. (2023). Power performance and motion response of a floating wind platform and multiple heaving wave energy converters hybrid system. *Energy*, 265, 126314.

[13] Mei, C. C., Stiassnie, M. A., & Yue, D. K. P. (2005). Theory and applications of ocean surface waves: Part 1: linear aspects. World Scientific.

[14] Madhi, F., Sinclair, M. E., & Yeung, R. W. (2014). The "Berkeley Wedge": an asymmetrical energy-capturing floating breakwater of high performance. *Marine Systems & Ocean Technology*, 9(1), 5-16.

[15] He, F., Zhang, H., Zhao, J., Zheng, S., & Iglesias, G. (2019). Hydrodynamic performance of a pile-supported OWC breakwater: An analytical study. *Applied Ocean Research*, 88, 326-340.

[16] Chen, Q., Zang, J., Birchall, J., Ning, D., Zhao, X., & Gao, J. (2020). On the hydrodynamic performance of a vertical pile-restrained WEC-type floating breakwater. *Renewable Energy*, 146, 414-425.

[17] Zhou, B., Zhang, Q., Jin, P., Li, Y., Liu, Y., Zheng, S., & Ning, D. (2022). Geometric asymmetry in the energy conversion and wave attenuation of a power-take-off-integrated floating breakwater. *Ocean Engineering*, 246, 110576.

[18] He, F., Zhang, Y., Jiang, H., & Huang, C. (2023). Numerical investigation of solitary wave breaking over a slope based on multi-phase smoothed particle hydrodynamics. *Physics of Fluids*, 35(2), 023313.

[19] Zhou, B., Zheng, Z., Zhang, Q., Jin, P., Wang, L., & Ning, D. (2023). Wave attenuation and amplification by an abreast pair of floating parabolic breakwaters. *Energy*, 271, 127077.

[20] He, F., Li, J., Pan, J., & Yuan, Z. (2023). An experimental study of a rectangular floating breakwater with vertical plates as wave-dissipating components. *Applied Ocean Research*, 133, 103497.

[21] Ren, J., Jin, P., Liu, Y., & Zang, J. (2021). Wave attenuation and focusing by a parabolic arc pontoon breakwater. *Energy*, 217, 119405.

[22] Zhang, H., Zhou, B., Zang, J., Vogel, C., Jin, P., & Ning, D. (2021). Optimization of a three-dimensional hybrid system combining a floating breakwater and a wave energy converter array. *Energy Conversion and Management*, 247, 114717.

[23] Zhang, Y., Li, M., Zhao, X., & Chen, L. (2020). The effect of the coastal reflection on the performance of a floating breakwater-WEC system. *Applied Ocean Research*, 100, 102117.

[24] Sarkar, D., Renzi, E., & Dias, F. (2015). Effect of a straight coast on the hydrodynamics and performance of the oscillating wave surge converter. *Ocean Engineering*, 105, 25-32.

[25] Zhang, H., Zhou, B., Vogel, C., Willden, R., Zang, J., & Geng, J. (2020). Hydrodynamic performance of a dual-floater hybrid system combining a floating breakwater and an oscillating-buoy type wave energy converter. *Applied Energy*, 259, 114212.

[26] Isaacson, M., & Qu, S. (1990). Waves in a harbour with partially reflecting boundaries. Coastal Engineering, 14(3), 193-214.

[27] Berkhoff, J. C. W. (1976). Mathematical models for simple harmonic linear water waves: wave diffraction and refraction. *Ph. D. Thesis*.

[28] Elchahal, G., Younes, R., & Lafon, P. (2008). The effects of reflection coefficient of the harbour sidewall on the performance of floating breakwaters. *Ocean Engineering*, 35(11-12), 1102-1112.

[29] Zhao, X., Du, X., Li, M., & Göteman, M. (2021). Semi-analytical study on the hydrodynamic performance of an interconnected floating breakwater-WEC system in presence of the seawall. *Applied Ocean Research*, 109, 102555.

[30] Ning, D. Z., Zhao, X. L., Zhao, M., Hann, M., & Kang, H. G. (2017). Analytical investigation of hydrodynamic performance of a dual float WEC-type breakwater. *Applied Ocean Research*, 65, 102-111.

[31] Goda, Y. (2010). Random seas and design of maritime structures (Vol. 33). World Scientific Publishing Company.

[32] Newman, J. N. (2018). Marine Hydrodynamics (p. 448). The MIT Press, Cambridge, Mass.

[33] Zheng, Y. H., Shen, Y. M., You, Y. G., Wu, B. J., & Jie, D. S. (2004). On the radiation and diffraction of water waves by a rectangular structure with a sidewall. *Ocean Engineering*, 31(17-18), 2087-2104.

[34] Zheng, Y. H., You, Y. G., & Shen, Y. M. (2004). On the radiation and diffraction of water waves by a rectangular buoy. *Ocean Engineering*, 31(8-9), 1063-1082.

[35] Mei, C. C. (1989). The Applied Dynamics of Ocean Surface Waves. World Scientific, Singapore.

[36] Falnes, J. & Kurniawan, A. (2020). Ocean Waves and Oscillating Systems: Linear Interactions

Including Wave-Energy Extraction. Cambridge University Press, UK.

[37] Holthuijsen, L. H. (2010). Waves in Oceanic and Coastal Waters. *Cambridge University Press*, UK.

[38] Sun, S. Y., Sun, S. L., & Wu, G. X. (2018). Fully nonlinear time domain analysis for hydrodynamic performance of an oscillating wave surge converter. *China Ocean Engineering*, 32(5), 582-592.

[39] Hu, J., Zhou, B., Vogel, C., Liu, P., Willden, R., Sun, K., ... & Collu, M. (2020). Optimal design and performance analysis of a hybrid system combing a floating wind platform and wave energy converters. *Applied Energy*, 269, 114998.